ISSN 1063-7761, Journal of Experimental and Theoretical Physics, 2019, Vol. 128, No. 4, pp. 630–640. © Pleiades Publishing, Inc., 2019.
Russian Text © V.A. Dudnikov, N.V. Kazak, Yu.S. Orlov, S.N. Vereshchagin, S.Yu. Gavrilkin, A.Yu. Tsvetkov, M.V. Gorev, A.A. Veligzhanin, A.L. Trigub, I.O. Troyanchuk, S.G. Ovchinnikov, 2019, published in Zhurnal Eksperimental'noi i Teoreticheskoi Fiziki, 2019, Vol. 155, No. 4, pp. 737–749.

ORDER, DISORDER, AND PHASE TRANSITION IN CONDENSED SYSTEM

Structural, Magnetic, and Thermodynamic Properties of Ordered and Disordered Cobaltite $Gd_{0.1}Sr_{0.9}CoO_{3-\delta}$

V. A. Dudnikov[a], N. V. Kazak[a], Yu. S. Orlov[a, b,*], S. N. Vereshchagin[c], S. Yu. Gavrilkin[d], A. Yu. Tsvetkov[d], M. V. Gorev[a], A. A. Veligzhanin[e], A. L. Trigub[e], I. O. Troyanchuk[f], and S. G. Ovchinnikov[a, b]

[a] *Kirensky Institute of Physics, Siberian Branch, Russian Academy of Sciences, Krasnoyarsk, 660036 Russia*

[b] *Siberian Federal University, Krasnoyarsk, 660041 Russia*

[c] *Institute of Chemistry and Chemical Technology, Siberian Branch, Russian Academy of Sciences, Krasnoyarsk, 660036 Russia*

[d] *Lebedev Physical Institute, Russian Academy of Sciences, Moscow, 119991 Russia*

[e] *National Research Center Kurchatov Institute, Moscow, 123182 Russia*

[f] *Scientific and Practical Materials Research Center, National Academy of Sciences of Belarus, Minsk, 220072 Belarus*

** e-mail: jso.krasn@mail.ru*

Received September 5, 2018; revised September 5, 2018; accepted October 1, 2018

Abstract—The effect of cationic and anionic orderings on the crystal structure and magnetic properties of substituted rare-earth cobaltites $Gd_{0.1}Sr_{0.9}CoO_{3-\delta}$ was studied using X-ray diffraction, measurement of XANES spectra, and magnetic and thermodynamic characteristics. The effects of ordering cause a decrease in symmetry to tetragonal and a distortion of the coordination octahedra of CoO_6. Anomalous magnetic and thermodynamic quantities are observed at 260 and 360 K, respectively, for disordered and ordered samples. The XANES spectra measured at the Co*K* edge did not reveal a noticeable shift in the absorption edge compared with the spectrum of original $GdCoO_3$. This suggests that the charge compensation process is associated not only with a change in the electronic state of cobalt ions, but also with the emergence of holes in the 2*p* states of oxygen.

DOI: 10.1134/S1063776119020171

1. INTRODUCTION

Perovskite-like rare-earth cobaltites $R_{1-x}A_xCoO_{3-\delta}$ (R is a rare-earth ion, A = Ba, Sr, Ca) belong to the family of strongly correlated electronic systems in which the relationship of different degrees of freedom leads to a rich phase diagram. Cobaltites exhibit cascades of structural and magnetic phase transitions as well as the metal–insulator transition, orbital ordering, and spin ordering. In compounds of this class there is a colossal magnetoresistance [1]. Depending on the concentration of alkaline earth element (x) and oxygen content (δ), cobalt ions can be in different charge and spin states and have different local environments (octahedral, pyramidal, tetrahedral).

The use of electron, X-ray and neutron diffraction together made it possible to determine the conditions for the formation of single-phase rare-earth-substituted cobaltites $Ln_{1-x}Sr_xCoO_{3-\delta}$ (Ln = Ln^{3+}–Yb^{3+}) and detect complex tetragonal and orthorhombic superstructures with properties defined by the type of cation and oxygen deficiency [2–5]. When $Ln_{1-x}Sr_xCoO_{3-\delta}$ perovskites are formed, a different equilibrium distributions of the Sr^{2+} and Ln^{3+} ions are possible depending on the ratio of the ionic radii of the cations. For all Ln = La–Nd elements, the structure with a completely disordered distribution of Sr^{2+}/Ln^{3+} cations at the crystallographic A positions is stable at all temperatures. For elements whose radius is smaller than that of Nd^{3+}, disordered perovskites exist at high temperatures; the structure with an ordered arrangement of Sr^{2+}, Ln^{3+} cations and anion vacancies is stable at low temperatures [2, 3]. These disordered $Ln_{1-x}Sr_xCoO_{3-\delta}$ perovskites can be obtained in the form of metastable phases by quenching high-temperature states [6]. Many works [7–10] are devoted to the study of ordered/disordered perovskites. However, the study of the effect of order–disorder transitions on the properties of materials is usually limited to the ordering of oxygen vacancies in the anion sublattice, and a comparative analysis of the physical and chemical properties for different cation distributions in the A position is quite rare. In the parent composition of $GdCoO_3$,

Co^{3+} ions are nonmagnetic in the ground state ($t_{2g}^6 e_g^0$ LS, $S = 0$). With increasing temperature or in the case of crystal lattice deformation caused by negative pressure, the spin state of cobalt ions may change, that is, low-lying excited states are gradually populated ($t_{2g}^4 e_g^2$ HS, $S = 2$). Estimates of the spin gap (the excitation energy of the HS state from the LS state at $T = 0$ K) in $GdCoO_3$ gave a value of 2300 K [11, 12]. Below the Néel temperature $T_N = 3.3$ K, the magnetic moments of Gd^{3+} ions are antiferromagnetically ordered.

The partial substitution of Sr^{2+} ions (ionic radius, 1.44 Å, coordination number $z = 12$) for Gd^{3+} ions (ionic radius 1.215 Å, $z = 12$) [13] leads to an increase in the unit cell volume V. At room temperature $V = 210.23$ Å^3 for $GdCoO_3$ and $V = 218.39$ Å^3 for $Gd_{0.4}Sr_{0.6}CoO_{2.85}$ [14]. This leads to a decrease in chemical pressure, thereby reducing the crystal field and the spin gap. In contrast to the stabilized low-spin state of Co^{3+} ions in $GdCoO_3$ for temperatures below room temperature, the spin states of cobalt ions in the case of $Gd_{1-x}Sr_xCoO_{3-\delta}$ compositions, the question of is not fully studied. The use of the Birch–Murnaghan equation of state for estimating the spin gap in $GdCoO_3$ [11] and in $La_{1-x}Gd_xCoO_3$ solid solutions [12] made it possible to calculate the chemical pressure created by lanthanoid compression below which a high-spin cobalt state may exist at room temperature [15]. The obtained value of this pressure (about 7 GPa) corresponds to the unit cell volume of the perovskite $V = 213.88$ Å^3. This makes it possible to suggest that for doped cobaltites $Gd_{1-x}Sr_xCoO_{3-\delta}$ in the case of the octahedral environment, part of the Co^{3+} ions in the $Gd_{1-x}Sr_xCoO_{3-\delta}$ compounds may be in the HS state at lower temperatures.

The goal of this work is to study the influence of ordering effects in the cation and anion sublattices on the crystal structure and magnetic and thermodynamic properties of the $Gd_{0.1}Sr_{0.9}CoO_{3-\delta}$ system.

2. SAMPLES AND EXPERIMENTAL TECHNIQUE

The polycrystalline $Gd_{0.1}Sr_{0.9}CoO_{3-\delta}$ (GSC) samples with perovskite structure were prepared using conventional ceramic technology from a stoichiometric mixture of Co_3O_4 (99.7%, metals basis), Gd_2O_3 (99.99%, REO) and $SrCO_3$ (99.99%, metals basis) oxides which have been preliminarily mixed thoroughly in an agate mortar with ethanol. The resulting mixture was annealed at a temperature of $T_s = 1473$ K in a platinum crucible for 24 h in air with multiply repeated grinding and calcination cycles. The rate of subsequent cooling affected the formation of ordered and disordered structures. The cation-ordered perovskite structure (GSC-ord) was obtained by slow cooling at a rate of 2 K/min, whereas a disordered structure (GSC-dis) was formed with rapid cooling (quenching) at a rate of 30 K/s and higher. To stabilize the oxygen content and its uniform distribution over the bulk, the samples were kept at 773 K in air for 24 h.

X-ray diffraction analyzes were performed using a PANalytical X'Pert PRO powder diffractometer (Netherlands, CoK_α); the measurements were performed using an Anton Paar HTK 1200N high-temperature camera (Anton Paar, Austria) over the range of angles of $2\theta = 10°–140°$. The lattice parameters were determined from the positions of the diffraction maximums using the ITO software [16]. The crystal structure was refined using the full-profile diffraction pattern using the Rietveld method [17] and the method of difference derivative minimization [18].

The oxygen content and the nonstoichiometry index δ were determined by the mass loss (Δm, %) [19] using a NETZSCH STA 449C analyzer equipped with an Aeolos QMS 403C mass spectrometer. The value of Δm was measured during sample recovery in the flow of a 5% H_2–Ar mixture when heated to 1127 K at a rate of 10 K/min assuming that cobalt is reduced to a metallic state. The values of $\delta = 0.35 \pm 0.01$ for the ordered (GSC-ord) and $\delta = 0.27 \pm 0.01$ for the disordered (GSC-dis) compositions were obtained.

X-ray absorption near edge structure (XANES) and extended X-ray absorption fine structure (EXAFS) spectra were measured on the K edge of Co and L_3 edge of Gd at the STM (K1.3b) station at the National Research Center Kurchatov Institute. The absorption spectra were recorded in transmission geometry at room temperature. A single crystal monochromator with a Si(111) slot was used that provided an energy resolution of $\Delta E/E \approx 2 \times 10^{-4}$. The XANES scanning was approximately 0.4 eV. The signal accumulation lasted 4 s per each point. The heat capacity of the samples was calculated from digital selective calling (DSC) curves by the method of proportions, Eq. (1), using a sapphire disk as a standard. The measurements were carried out in a platinum crucible with a perforated lid in a flow of a 20% O_2–Ar mixture. The heating rate was 10 K/min. The presented results are the average of three independent measurements.

$$C_P = \frac{m_{st}}{m_{sa}} \frac{\mathrm{DSC}_{sa} - \mathrm{DSC}_{bl}}{\mathrm{DSC}_{st} - \mathrm{DSC}_{bl}} C_{P,st}, \quad (1)$$

where C_P is the heat capacity of the sample at temperature T, $C_{P,st}$ is the tabulated heat capacity of a standard sample (sapphire) at temperature T, m_{st} and m_{sa} are standard and sample masses, DSC_{sa}, (DSC_{st}, DSC_{bl}) are at the level of the DSC signal of the sample (standard, zero line) at temperature T. Measurements were performed in a temperature range of 320–450 K.

Thermal expansion was studied at 100–700 K using a NETZSCH DIL 402 C induction dilatometer in the dynamic mode with heating and cooling rates of 3 K/min with purging by dry helium (a O_2 content of about 0.05 vol %). The rod load on the sample was

0.3 N. For calibration and taking into account the expansion of the measuring system, fused quartz standards were used.

The measurements of the temperature and field dependences of the magnetization in the temperature range from 2 to 400 K were carried out using a universal PPMS-9 setup (Physical Properties Measurement System, Quantum Design, USA), equipped with special modules for these types of measurements at the Center of Collective Use of Lebedev Physical Institute (Moscow).

3. RESULTS

3.1. X-ray Diffraction

X-ray diffraction did not reveal the presence of extraneous phases. Analysis of the crystal structure showed that the samples subjected to quenching (rapid cooling) have cubic crystal symmetry, and samples obtained by slow cooling have tetragonal symmetry as indicated by the appearance of additional superstructural reflexes (Fig. 1). The lattice parameters of the samples are given in Table 1. At a temperature of synthesis T_s = 1473 K, the $Gd_{0.1}Sr_{0.9}CoO_{3-\delta}$ sample is a cubic perovskite phase with a uniform random distribution of Sr^{2+}/Gd^{3+} and anion vacancies in the corresponding positions of the crystal lattice.

In rapid cooling, a random uniform Sr^{2+}/Gd^{3+} distribution is frozen in the crystal lattice with the formation of a metastable single-phase material with a cubic structure (GSC-dis) (Fig. 2a). In slow cooling in a temperature range of 1473–1173 K, an ordered low symmetry phase (GSC-ord) is formed due to partial ordering of the Sr^{2+}/Gd^{3+} cations and anion vacancies (Fig. 2b). The disorder–order transition is accompanied by an endothermic peak on the DSC curves (Fig. 2c). The transition temperature was defined as $T_{dis-ord}$ = 1263 K. When $Gd_{0.1}Sr_{0.9}CoO_{3-\delta}$ samples are heated in an oxidizing atmosphere (in air), the reversible oxygen abstraction is observed, and the heating/cooling processes are accompanied by structural and chemical changes manifested in the form of effects on DSC curves.

In the GSC-dis cubic lattice, all A positions are crystallographically equivalent and randomly occupied by Gd/Sr atoms. The distribution of oxygen vacancies is random. In the tetragonal-distorted perovskite GSC-ord, ordering leads to the appearance of two nonequivalent positions A1 and A2, the first of which is occupied by a mixture of Gd/Sr atoms in a ratio of 0.1/0.4 and the second, by Sr atoms. Cobalt ions occupy two nonequivalent positions, Co1 and Co2. Oxygen atoms have four nonequivalent positions, of which O3 and O4 are the localization of oxygen vacancies, which are mainly concentrated in the O3 position.

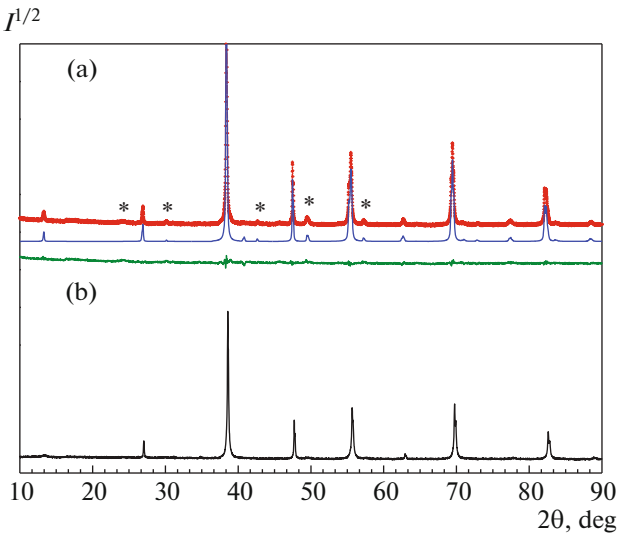

Fig. 1. Experimental (red), calculated (blue), and difference (green) X-ray patterns of the ordered composition $Gd_{0.1}Sr_{0.9}CoO_{2.65}$ (a) and experimental X-ray pattern (black) of the disordered composition $Gd_{0.1}Sr_{0.9}CoO_{2.74}$ (b). Superstructural reflexes of tetragonal perovskite are shown by an asterisk.

The atomic coordinates and the occupancies of nonequivalent crystallographic positions and the parameters of isotropic displacement for the cation-ordered cobaltite $Gd_{0.1}Sr_{0.9}CoO_{2.65}$ are given in Table 2. The individual interionic distances are given in Table 3. Oxygen octahedra $Co1O_6$ and $Co2O_6$ have characteristic tetragonal distortions. The $Co1O_6$ octahedron is compressed in the *ab* plane and stretched along the *c* axis, while the $Co2O_6$ octahedron, on the contrary, is compressed along the *c* axis and has a significant elongation of bonds in the *ab* plane.

Thus, an ordered perovskite has a structure consisting of layers located along the *c* axis in the sequence $[Sr_{0.5}O_{0.5}]$–$[Co_{0.5}O]$–$[Gd_{0.1}Sr_{0.4}O_{0.5-0.4\delta}]$–$[Co_{0.5}O_{1-0.6\delta}]$. Tetragonal distortions in the structure of the ordered composition of GSC-ord are probably associated with

Table 1. Parameters of the crystal lattice of cobaltites

Compound	Space group	*a*, Å	*b*, Å	*c*, Å	*V*, Å^3
$GdCoO_3$	*Pbnm* (62) orthorhombic	5.2259	5.391	7.4556	210.05
$Gd_{0.1}Sr_{0.9}CoO_{2.74}$ (dis)	*Pm* – 3*m* (221) cubic	3.8462	–	–	56.898
$Gd_{0.1}Sr_{0.9}CoO_{2.65}$ (ord)	*P*4*mm* (99) tetragonal	3.8428	–	7.7203	114.001

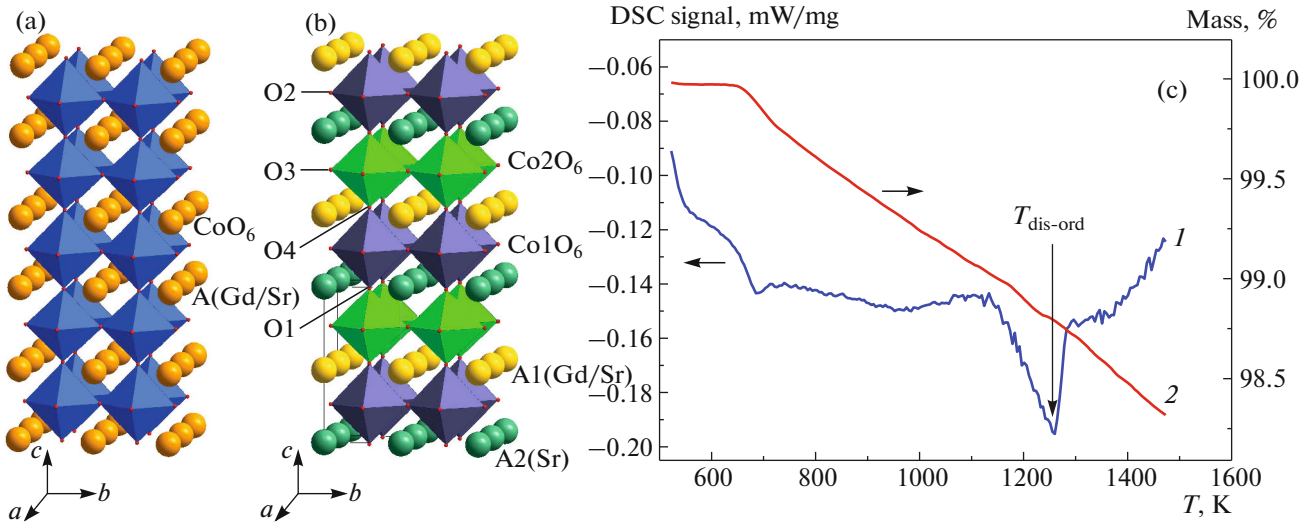

Fig. 2. Crystal structure of perovskites: (a) $Gd_{0.1}Sr_{0.9}CoO_{2.74}$ with a disordered distribution of Gd/Sr atoms over the A positions (GSC-dis); (b) $Gd_{0.1}Sr_{0.9}CoO_{2.65}$ with an ordered distribution (GSC-ord). For the tetragonal structure, the nonequivalent positions of cobalt Co1 and Co2 are shown by the violet and green octahedra, respectively. The red color shows the nonequivalent positions of oxygen, among which O3 and O4 correspond to the predominant localization of oxygen vacancies. (c) Temperature dependences of the DSC (*1*) signal and mass (*2*) for sample $Sr_{0.9}Gd_{0.1}Co_{3-\delta}$; conditions: dynamic 20% O_2–Ar atmosphere; sample weight, 27 mg, a platinum crucible with perforated lid; heating rate, 10 K/min.

the regular position of Gd/Sr atoms and oxygen in the lattice and, as a result, with the consistent ordering of local structural distortions.

The removal of oxygen changes the local environment of two neighboring Co^{3+} ions from octahedral to pyramidal. The concentration of CoO_5 complexes reaches 52% in the disordered GSC-dis sample and 70% in the ordered GSC-ord sample. The formation of oxygen vacancies causes a change in the Co–Co interionic distance. Thus, in the ordered GSC-ord sample, a decrease in the Co–Co distance along the *c* axis, which is the Co1– O4–Co2 bond length, is associated with the removal of apical O4 oxygen. The crystal field of Co^{3+} ions in the pyramidal environment should be less split thus reducing the concentration of the LS state of cobalt in the crystal.

Table 2. Atomic coordinates, isotropic displacement parameter *U*, and the site occupancy factors (s.o.f.) for the cation-ordered $Gd_{0.1}Sr_{0.9}CoO_{2.65}$ perovskite

Atom	*x/a*	*y/b*	*z/c*	*U*, Å^2	S.O.F.
Sr1	0	0.0	0.46321	0.0118	0.4
Gd1	0	0.0	0.51164	0.0118	0.1
Sr2	0	0.0	0.00000	0.0152	0.5
Co1	0.5	0.5	0.24670	0.0069	0.5
Co2	0.5	0.5	0.72886	0.0130	0.5
O1	0.5	0.5	−0.02969	0.0287	0.5
O2	0.5	0.0	0.22167	0.0241	1.0
O3	0.5	0.0	0.72761	0.0189	0.6376
O4	0.5	0.5	0.48831	0.0850	0.4224

At the same level of substitution, ordering leads to two different cooperative effects. First, the distribution of anionic vacancies over lattice sites causes order (disorder) associated with the octahedral and pyramidal environment of cobalt ions. In the GSC-ord sample, the concentration of oxygen vacancies in the O3 position is 1.5 times higher than in the O4 position. Such a distribution of vacancies in neighboring layers leads to the uneven appearance of cobalt ions with the pyramidal environment of CoO_5. The probability of such coordination significantly increases for cobalt ions in the Co2 position, for which there is also some probability of CoO_4 tetrahedral coordination, since two oxygen atoms (O3 and O4) out of six may be vacant.

The second effect is that structural changes affect the remaining Co^{3+} ions in octahedral coordination. The partial substitution of Sr ions for Gd ions leads to the greater distortion of oxygen octahedra. As can be seen from the Table 3, structural changes in ordered and disordered samples are not the same. Despite the fact that the mean interionic distances ⟨Co–O⟩ are close, the ⟨Co–Co⟩ distance greatly increases for an ordered sample and is significantly greater than hat in unsubstituted cobaltite $GdCoO_3$. This is due to an increase in the Co–O–Co bond angle, which approaches an ideal value of 180° in cubic structures (Fig. 3). A better alignment of cobalt ions along the magnetic coupling favors the overlapping of the electronic Co(3*d*) and O(2*p*) orbitals and the enhancement of the exchange interaction.

Table 3. Individual and average interionic distances (in angstroms) and the bond angle (in degrees) in the $GdCoO_3$ and $Gd_{0.1}Sr_{0.9}CoO_{3-\delta}$ perovskites

$GdCoO_3$		$Gd_{0.1}Sr_{0.9}CoO_{2.65}$ (ord)				$Gd_{0.1}Sr_{0.9}CoO_{2.74}$ (dis)	
Co–O1	2 × 1.9193	Co1–O1	1 × 2.1338	Co2–O1	1 × 1.8641	Co–O	6 × 1.924
Co–O2	2 × 1.9357	Co1–O4	1 × 1.8653	Co2–O4	1 × 1.8571		
	2 × 1.9422	Co1–O2	1 × 1.9311	Co2–O3	1 × 1.9214		
⟨Co–O⟩	1.9324	1.9275				1.9246	
Co–Co (plane)	4 × 3.7541	4 × 3.8428				3.8336	
Co–Co (axis *c*)	2 × 3.7278	1 × 3.7224				3.8336	
		1 × 3.9979					
⟨Co–Co⟩	3.7453	3.8485				3.8336	
Co–O–Co (plane)	151°	169°		179°		170°	
Co–O–Co (axis *c*)	152°	180°				170°	
⟨Gd–O⟩	2.6857	⟨Gd1/Sr1–O⟩	2.6916	⟨Sr2–O⟩	2.7162	⟨Gd/Sr–O⟩	2.7136

3.2. XANES Spectroscopy

The normalized XANES spectra of the ordered $Gd_{0.1}Sr_{0.9}CoO_{2.65}$ and disordered $Gd_{0.1}Sr_{0.9}CoO_{2.74}$ samples recorded at room temperature at the Co*K* edge are presented in Fig. 4a in comparison with the $GdCoO_3$ spectra. For all spectra, there are three main features: the electronic transition from the cobalt 1*s* ground state to subbands constructed from hybridized Co(3*d*)–O(2*p*)–Co(4*p*) states (feature *A*) near the bottom of the conduction band and to bands with the dominant Co(4*p*) nature hybridized with the states O(2*p*) and split by the crystal field in the region of the main absorption maximum (features *B* and *C*). The energy positions of these features were determined from the minimum of the second derivative of the absorption coefficient $d^2\mu/dE^2$ shown in the lower inset of Fig. 4. The corresponding numerical values are presented in Table 4.

For $GdCoO_3$, the pre-edge feature *A* in a range of 7709–7712 eV is a doublet structure and corresponds to the $1s \rightarrow 3d$ transition, which is forbidden in the dipole approximation. This transition manifests itself due to the *d*/*p* orbital mixing and quadrupole contributions. The shape and intensity of the pre-edge features correlate with the degree of distortion of the coordination octahedron and are an indicator of the Co^{3+} ion in low-symmetry configurations (the relative intensity of this spectral component is especially high in the case of noncentrosymmetric configurations).

Two features clearly distinguishable in the second derivative (the lower inset in Fig. 4a) can be attributed to the splitting of the *d* states of cobalt by the crystal field of approximate octahedral symmetry into the t_{2g} and e_g components. The value of splitting (~2.6 eV) is close to that (2.3 eV) in $LaCoO_3$ [20]. Because the t_{2g} and e_g orbitals are not isolated states but form electron

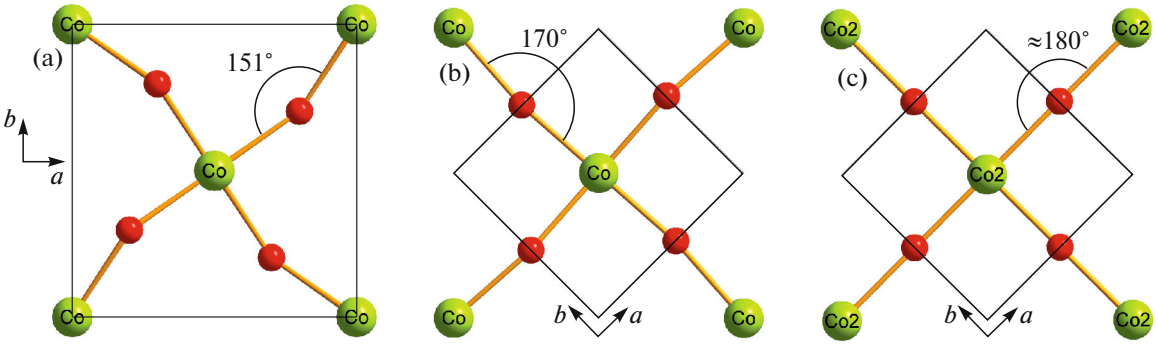

Fig. 3. Effect of substitution and ordering on the value of the Co–O–Co bond angle in the *ab* plane for the $GdCoO_3$ (a) GSC-dis (b), and GSC-ord (c) samples.

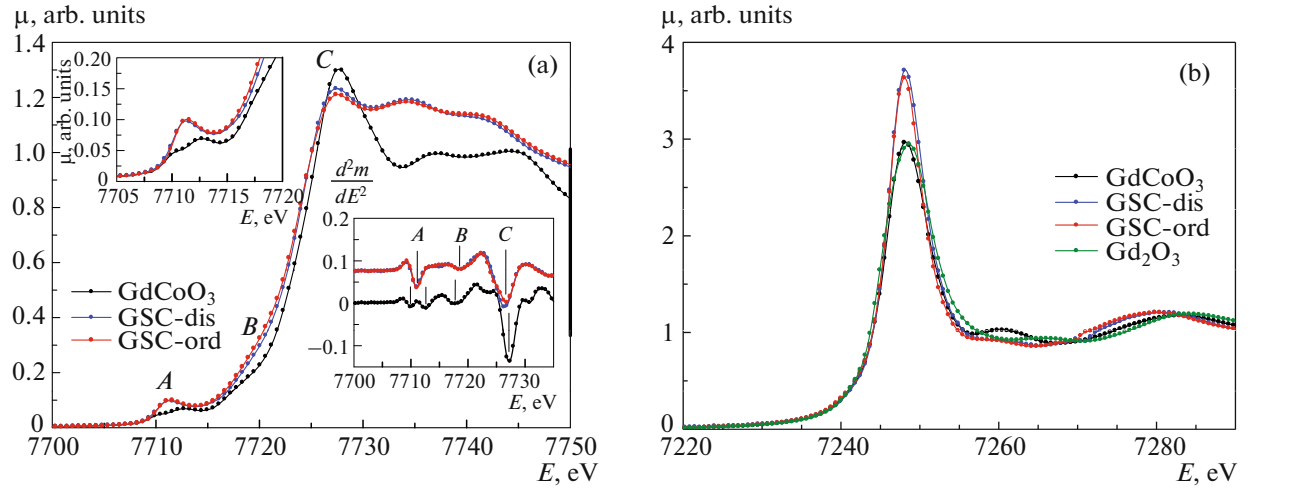

Fig. 4. XANES spectra of $GdCoO_3$ samples (black curves), $Gd_{0.1}Sr_{0.9}CoO_{3-\delta}$ measured at the CoK edge (a) and GdL_3 edge (b). The upper inset is the pre-edge feature on an enlarged scale. The lower inset is the second derivative of the XANES spectrum.

zones with occupancies varying with temperature, the states with different spin configurations can overlap at a given temperature.

The spectral feature *C* at 7727 eV (Fig. 4a) corresponds to the dipole-allowed main transition $1s \rightarrow 4p$ for Co^{3+}. Note that the energy positions of the spectral features in $GdCoO_3$ are slightly shifted toward higher energies compared to $LaCoO_3$. For example, the absorption edge of Co^{3+} determined from the maximum of the first derivative is 7725.7 eV in the first compound and 7724 eV in the second. In this case, the energy difference between the corresponding features is preserved. Thus, the energy difference between the $1s \rightarrow e_g$ and $1s \rightarrow 4p$ transitions in $GdCoO_3$ is 14.9 eV, which agrees well with the XANES data (14.3–14.9 eV) for other rare-earth cobaltites $RCoO_3$ (R = La, Ho, Gd, Nd) [21].

In the XANES spectrum of $GdCoO_3$ (Fig. 4a), a shoulder is observed near 7718 eV (feature *B*). It can be assumed that this feature is related to the process of ligand-to-metal charge transfer (LMCT), when there is a multielectron transition $\underline{1s}\,3d^{n+1}4p^1\underline{L}^1$ with charge transfer from the ligand to the levels of Co (3*d*) in addition to the direct transition $\underline{1s}\,3d^n4p^1L^2$. These transitions are lower in energy than the main transition, and their intensity depends on the degree of covalence of this site. It is important to note that the direct overlap between Co(3*d*) orbitals is small in the perovskite structure and O(2*p*) oxygen orbitals, which directly participate in indirect exchange interaction, can contribute to O(2*p*) → Co(3*d*) transitions with charge transfer. In the second derivative of the $GdCoO_3$ XANES spectrum near 7723 eV (the lower inset in Fig. 4a) a well resolved minimum is seen. A fine structure of this sort was observed in the XANES spectra of $LaCoO_3$ and was attributed to Co(1*s*) → Co(4*sp*) hybrid transitions.

Table 4. Electronic transition energies (in electronvolts), determined from XANES spectra of $GdCoO_3$ and $Gd_{0.1}Sr_{0.9}CoO_{3-\delta}$ cobaltites

	$GdCoO_3$	$Gd_{0.1}Sr_{0.9}CoO_{3-\delta}$
A	7709.9	7711.1
	7712.5	
B	7717.8	7718.7
C	7727.4	7726.6

The spectra of the substituted samples are similar in shape but differ from those of $GdCoO_3$ in the intensity and energy positions of the spectral features. In the substituted compositions $Gd_{0.1}Sr_{0.9}CoO_{3-\delta}$, the shape and intensity of the pre-edge feature *A* is very different from that in $GdCoO_3$, which may indicate a mixed coordination of cobalt ions with oxygen ions. In the main XANES absorption region, the spectra of substituted samples slightly shift toward lower energies, and the intensity of the main transition (*C*) decreases compared with the case of $GdCoO_3$. A similar effect was previously observed in the $Dy_{1-x}Ca_xCoO_{3-\delta}$ system and was attributed to a change in the covalence of the Co–O bond [22]. Nevertheless, the energy position of the center of gravity of the doublet structure of the $1s \rightarrow 3d$ transition in $GdCoO_3$ (~7711.2 eV) agrees well with the position of maximum of the pre-edge feature in the substituted samples (~7711.1 eV), see the upper inset to Fig. 4a. This indicates that the formal valence of cobalt in the substituted samples is close to +3, i.e., the change in the positive charge caused by the substitution of Sr^{2+} does not lead to the appearance of Co^{4+}

Table 5. The magnetic parameters of substituted $Gd_{0.1}Sr_{0.9}CoO_{3-\delta}$ cobaltites

	μ_{eff}^{exp}, (μ_B/formula unit)	μ_{eff}^{extra}, (μ_B/formula unit)	Θ_{LT}, K	T_N, T_f, K	M_r, (μ_B/formula unit)	χ, μ_B/formula unit/Oe
$GdCoO_3$	7.33	–	−6.34	3.3	5.80	11.65×10^{-6}
$Gd_{0.1}Sr_{0.9}CoO_{2.74}$-dis	3.09	1.80	−5.33	250	0.62	2.08×10^{-6}
$Gd_{0.1}Sr_{0.9}CoO_{2.65}$-ord	2.88	1.41	−2.97	362	0.65	1.66×10^{-6}

states and should be compensated mainly by oxygen vacancies and by the appearance of "electron" holes on O(2*p*) states. In the energy range 7715–7720 eV (feature *B*), the spectral density of the substituted compositions is much higher than for $GdCoO_3$. In the second derivative of the absorption function, a well-resolved minimum is seen at 7718.7 eV, which is probably associated with the LMCT process. A shift toward higher energies and an increase in the intensity of this low-energy transition compared to $GdCoO_3$ can contribute to the main absorption edge and effectively shift it toward lower energies.

Note that a change in the symmetry of the nearest environment without a noticeable change in the Co–O distance will lead to a change in the XANES spectrum due to multiple scattering. The difference in the energy position of the spectral features can be an indicator of the difference in the degree of orbital mixing. The absence of one of the oxygen atoms in the nodes (compared to an octahedron) leads to a change in the hybridization between the O(2*p*) and $e_g(3z^2 - r^2)$ orbitals of the pyramidal Co. At the same time, a change in the Co–O–Co bond angle in the octahedral complex should cause a change in the degree of overlap of Co(3*d*) and O(2*p*) electron orbitals with the π bond.

The normalized XANES spectra of cobaltites obtained on the GdL_3 edge are shown in Fig. 4b together with the spectrum of Gd_2O_3. A maximum of about 7248 eV is associated with the $2p_{3/2} \rightarrow 5d$ dipole transition of the Gd^{3+} ion ($4f^7$). In contrast to 3*d* orbitals, the 4*f* orbitals of Gd are localized near the nucleus and poorly mixed with ligand *p* orbitals. As a result, their interaction with ligands has a small chemical consequence (the absence of shift of the absorption edge). Nevertheless, a change in the degree of overlap of Re(5*d*) and O(2*p*) orbitals and (or) an increase in the density of vacant O(2*p*) states can appear in the XANES spectra as changes in the intensities of the main transition.

3.3. Magnetism

The temperature dependences of the magnetization of a series of $Gd_{0.1}Sr_{0.9}CoO_{3-\delta}$ samples measured in cooling modes in the absence of a magnetic field (ZFC) and in the presence of a magnetic field (FC) are shown in Fig 5. For both compositions, with a decrease in temperature below the critical one (T_{div}^{dis} = 256 K for the GSC-dis composition and T_{div}^{ord} = 368 K for the GSC-ord composition), there is a hysteresis of the $M(T)$ dependences in the ZFC and FC modes. In the case of an ordered GSC-ord composition, the appearance of hysteresis is accompanied by a pronounced anomalous magnetization in the form of a maximum on the ZFC curve at 362 K and a sharp increase in the FC magnetization. Such a behavior is characteristic of systems whose magnetization contains a ferromagnetic (FM) component. In the high-temperature (HT) range at $T > 300$ K, the magnetization behavior of the disordered sample GSC-dis obeys the Curie–Weiss law with an effective magnetic moment $\mu_{eff} = 4.16 \pm 0.01\mu_B$/formula units and the Curie paramagnetic temperature $\Theta_{HT} = 57 \pm 1$ K (Fig. 6). The positive Curie temperature indicates the predominance of the exchange FM interaction in the system. Unfortunately, the limited range of measurements prevented us from obtaining a similar approximation for an ordered GSC-ord sample. In the low-temperature LT phase ($T < 15$ K), a characteristic increase in the magnetic moment is observed due to the paramagnetic contribution of the Gd^{3+} subsystem (the inset in Fig. 6). The values of the magnetic moment and the paramagnetic Curie temperature obtained by processing the low-temperature magnetic susceptibility are given in Table 5. The table also shows the magnetic parameters of the $GdCoO_3$ parent composition, which are in good agreement with previously published data [23, 24].

The effective magnetic moment in Sr-substituted cobaltites is defined as

$$\mu_{eff} = \sqrt{0.1\mu_{Gd}^2 + \mu_{extra}^2},$$

where μ_{Gd} is the magnetic moment of the Gd^{3+} ions, μ_{extra} is an additional contribution to the magnetic moment associated with the magnetism of cobalt ions and oxygen holes. We estimated the value of the additional contribution, assuming that the spectroscopic splitting factor is $g = 2$ for Gd^{3+} ions. It is seen that the magnetic defects associated with charge compensation cause an increase in the magnetic contribution already at low temperatures. The paramagnetic Curie temperature is negative in all samples studied, which indi-

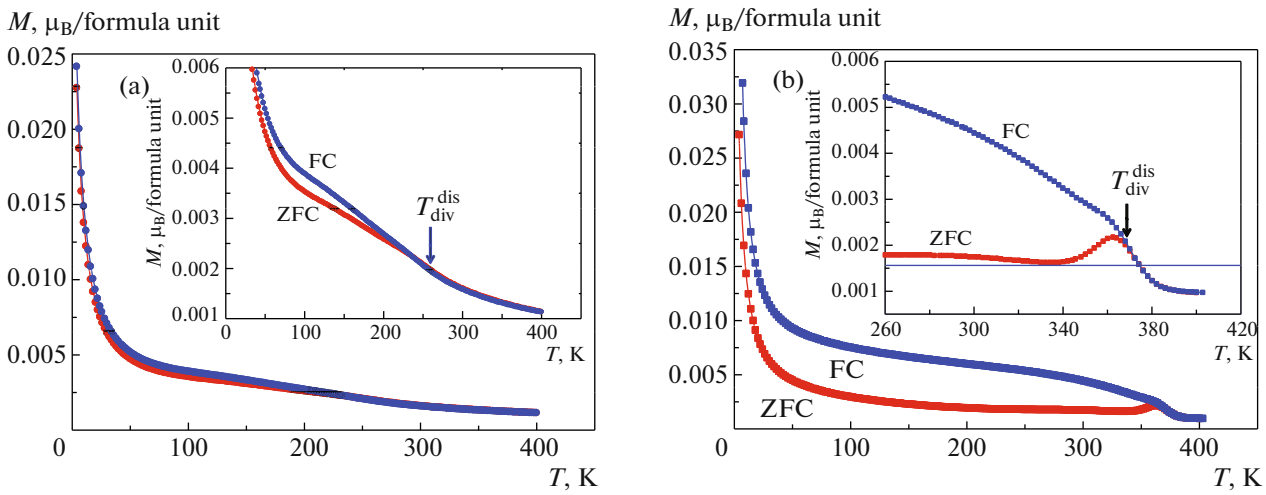

Fig. 5. Temperature dependences of the perovskite magnetization $Gd_{0.1}Sr_{0.9}CoO_{3-\delta}$ ((a) GSC-dis, (b) GSC-ord)) in ZFC modes (red curves) and FC (blue curves), $H = 1$ kOe. The arrows show the temperatures of the ZFC and FC magnetization curves.

cates the predominance of antiferromagnetic (AFM) interaction at low temperatures. The value of Θ_{LT} for an ordered composition is almost two times lower than for a disordered one. The weakened AFM interactions in a GSC-ord sample can be associated with both ordering effects (in GSC-ord, layers containing magnetic Gd atoms are spatially separated by layers of nonmagnetic Sr atoms) and an increase in the FM contribution due to the appearance of magnetic defects the B sublattice and magnetic holes.

The field dependences of the magnetization of the studied perovskites are shown in Fig. 7 At $T = 2$ K, in fields up to 50 kOe, a rapid increase in the magnetization is observed. Above 50 kOe, the magnetization depends linearly on the field and does not reach saturation even at $H = 90$ kOe. The residual magnetization M_r and magnetic susceptibility χ, determined from the linear portion of the $M(H)$ dependence in strong fields, are presented in Table 5. Taking into account the concentration of Gd ions in the substituted compositions, the M_r values found are close to the experimentally determined value for $GdCoO_3$ [23, 24].

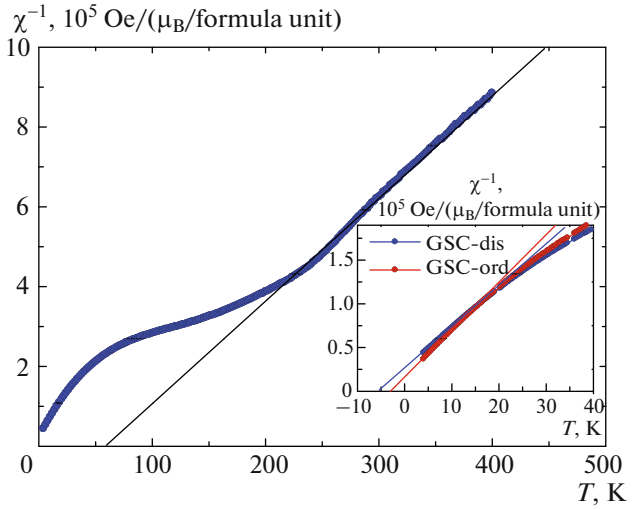

Fig. 6. Temperature dependence of the reciprocal magnetic susceptibility of the GSC-dis sample ($H = 1$ kOe). The inset shows the low-temperature part of the magnetic susceptibility of the GSC-ord and GSC-dis samples. Straight lines show approximation by the Curie–Weiss law.

Thus, the orientation of the magnetic moments of the Gd^{3+} ions in the direction of the external magnetic field occurs in fields of up to 50 kOe, then the magnetization process is associated with an additional magnetic contribution. The field dependences of magnetization $M(H)$ of an ordered GSC-ord sample in the region of magnetic transition are shown in Fig. 7b. At $T = 300$ K, there is a narrow, symmetrical hysteresis loop, which does not exhibit saturation. The value of the coercive force is $H_c = 0.46$ kOe. At $T = 350$ K, the shape of the loop is preserved, but the coercive force increases to ~1.0 kOe. Then, with an increase in temperature, the hysteresis loop transforms into a linear dependence characteristic of the paramagnetic state. Note that measurements of the field dependence of the magnetization of a disordered GSC-dis sample at these temperatures revealed paramagnetic behavior, which is in agreement with the temperature measurement data (not shown in the figure).

3.4. Heat Capacity and Thermal Expansion

The temperature dependences of the molar heat capacity of the ordered and disordered perovskites $Gd_{0.1}Sr_{0.9}CoO_{3-\delta}$ are presented in Fig. 8a. For GSC-ord at $T_M = 358$ K, a feature associated with the mag-

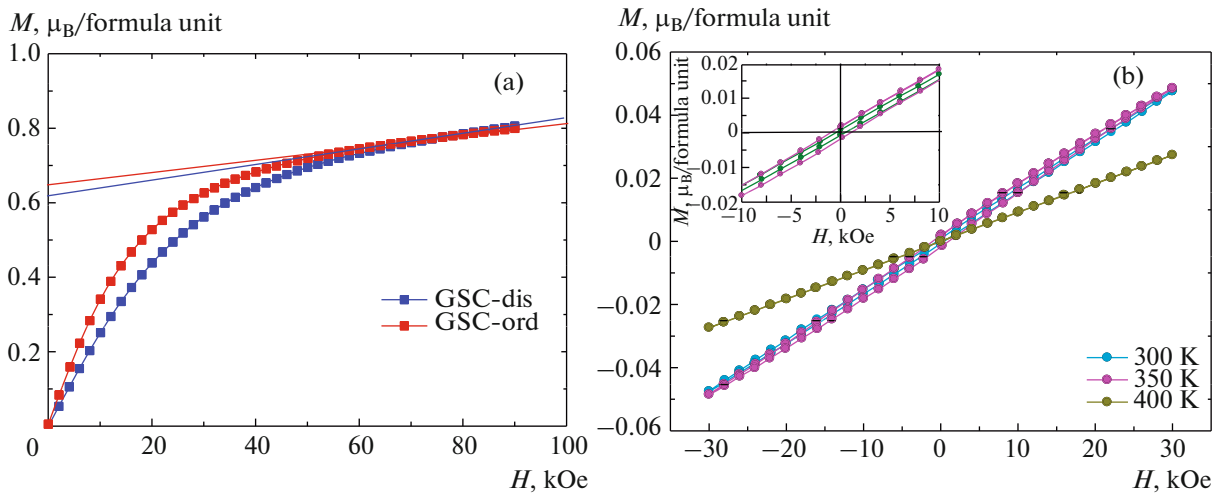

Fig. 7. Magnetization curves of $Gd_{0.1}Sr_{0.9}CoO_{3-\delta}$ samples at $T = 2$ K (a) and an ordered GSC-ord sample in the region of the magnetic transition (b). The inset shows the magnetization hysteresis loops at $T = 300$, 350 K.

netic transition is seen. The temperature dependences of thermal expansion $\Delta L/L$ are shown in Fig. 8b. With an increase in temperature, the volume of samples increases, which is due to the phonon anharmonic contribution. However, at $T_M = 260$ K and $T_M = 353$ K for GSC-dis and GSC-ord, respectively, there is a break associated with a change in the contribution to thermal expansion. These features are clearly seen in the temperature dependence of the thermal expansion coefficient shown in Fig. 8c. The T_M feature is more pronounced for the GSC-ord sample. A jump in the thermal expansion coefficient and the weak anomaly in the heat capacity at T_M correlate with magnetic measurements.

4. DISCUSSION

As a result of the partial substitution of Sr^{2+} ions for Gd^{3+} ions in cobaltites that are nonstoichiometric with respect to oxygen, oxygen vacancies and defects associated with the process of charge compensation are formed. The concentration of such defects depends on the ion subsystem they are formed in. If we assume that such defects are transition element ions (the appearance of Co^{4+} ions), their concentration is defined as $n(Co^{4+}) = x - 2\delta$ per formula units and for $\delta = x/2$ tends to zero. The concentration of such defects should reach 0.2 and 0.4 Co^{4+} per formula units in samples GSC-ord and GSC-dis, respectively. The Co^{4+} ion ($3d^5$) can be in three spin states: $t_{2g}^3 e_g^2$, $t_{2g}^4 e_g^1$, and $t_{2g}^5 e_g^0$, each being characterized by unpaired electrons and, therefore, has a magnetic moment.

The oxidation state of all elements in the compound is a nontrivial question. The X-ray absorption data of the $Gd_{0.1}Sr_{0.9}CoO_{3-\delta}$ samples under study indicate that the oxidation state of cobalt ions weakly depends on substitution. This should lead to the appearance of defects (holes) in the oxygen subsystem, the number of which is

$$n(O2p) = 2 - \frac{6 - x}{3 - \delta}.$$

In the studied compositions, the concentration of oxygen holes is defined as 0.08 and 0.14 per formula units for GSC-ord and GSC-dis, respectively. A hole on oxygen ($S = 1/2$) can act as an independent magnetic center or enter the composition of magnetic complexes.

Thus, Gd^{3+} ions, Co^{3+} ions in the octahedral coordination in the high-spin or intermediate spin (IS) state, Co^{3+} ions in a coordination different from the octahedral, and holes in the $O2p$ state can serve as sources of magnetism in the $Gd_{0.1}Sr_{0.9}CoO_{3-\delta}$ system, if charge compensation occurs in the oxygen sublattice. The Co^{4+} ions can also add to magnetism if the compensation process affects the transition element sublattice. It is hard to separate the contributions of each of these ions.

In the studied cobaltites with the same level of substitution ($x = 0.9$), the effects of ordering in different sublattices lead to unequal exchange disturbances. In this case, ordering may affect the magnetism of the $Gd_{1-x}Sr_xCoO_{3-\delta}$ system in several main ways. The first is reduced to the effect of diamagnetic dilution in the A sublattice when the partial exclusion of Gd^{3+} ions from the exchange leads to the spatial inhomogeneity of exchange. Since the interaction potential between the nearest Gd^{3+} ions changes with distance in proportion to r^{-3}, it can be expected that, in an ordered GSC-ord structure, where the magnetoactive Gd ions localized in layer A1 are spatially separated by

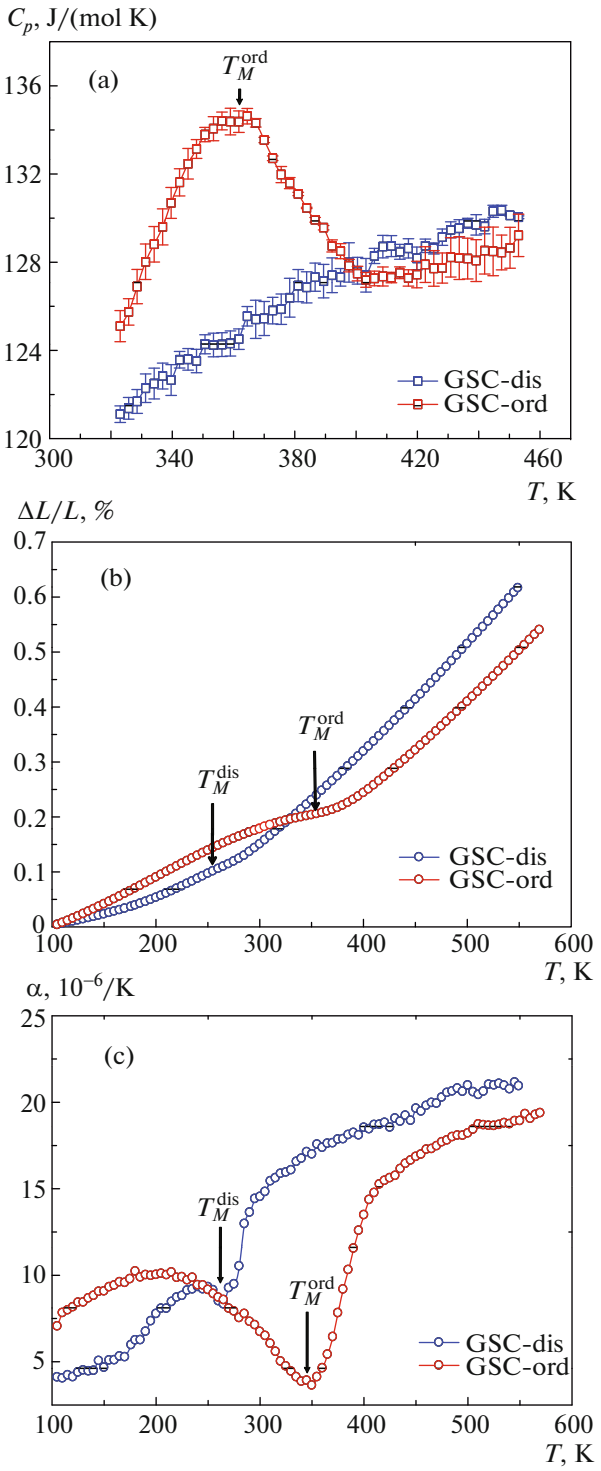

Fig. 8. Temperature dependences of the heat capacity (a), thermal expansion (b) and thermal expansion coefficient (c) of the ordered and disordered $Gd_{0.1}Sr_{0.9}CoO_{3-\delta}$ perovskites.

a layer of nonmagnetic ions A2 (Sr), the overlap of wave functions will be significantly smaller than in the case of a disordered GSC-dis sample, in which the Gd and Sr ions are randomly mixed in the A positions, thus increasing the probability of overlap. The weakening of the exchange coupling between the Gd ions is reflected in the decrease in the paramagnetic Curie temperature Θ_{LT} as determined from the analysis of low-temperature magnetic susceptibility. The second way assumes both the qualitative and quantitative influence of anionic ordering on the magnetic state of ions in the B sublattice. Quantitatively, the differences in the magnetic behavior of ordered and disordered compositions and as well as the values of freezing temperatures T_f of magnetic moments turned out to be the most noticeable. This is especially pronounced near magnetic transitions, where the enhancement of the FM contribution for the GSC-ord composition leads to a significant FC magnetization.

Oxygen vacancies and the associated magnetic states of Co^{3+} ions in the pyramidal environment act as inhomogeneities of the magnetic structure, in particular, cobalt ions in bipyramids [25], which at low temperatures can be in the IS or HS state [26], play an important role. In the case of the GSC-dis disordered composition, these inhomogeneities are randomly distributed over the lattice sites. The inhomogeneity manifest itself in the form of blurred $M(T)$ curves near the magnetic transition, which is pronounced for this sample. The $M_{ZFC(}T)$ curve has a wide correlation maximum, which shifts toward lower temperatures compared to the ordered GSC-ord sample. This behavior of magnetization is characteristic of systems in which there is a wide range of magnetic regions with the dispersion of exchange interaction intensities.

The freezing point of the magnetic moments of the FM regions, which is defined as a temperature corresponding to the maximum of the ZFC curve, is $T_f =$ 170 K. The greatest contribution to the magnetization is from the regions with the effective temperature $T_M =$ 250 K obtained from the maximum of the first derivative of the $M_{ZFC}(T)$ dependence. An increase in the degree of ordering of anion vacancies leads to the appearance of strongly correlated magnetic regions in which the spins are coupled ferromagnetically. The freezing point of magnetic moments T_f = 362 K can be reliably determined for the GSC-ord sample. Assuming that the value of T_f determines the average diameter of the FM clusters, we can state that an increase in T_f in the ordered sample indicates an increase in the average size of the FM clusters.

As a result of a systematic study of the crystal structure, magnetic and thermal properties of $Gd_{0.1}Sr_{0.9}CoO_{3-\delta}$ cobaltites, we the following findings. The ordering of anionic vacancies has a greater effect on the magnetic properties of the system and leads to an increase in ferromagnetism (an increase in the magnetic transition temperature and magnetic moment). The ordering in the A sublattice reduces to weaker Gd–Gd AFM interactions. This is due to the fact that the main interaction in the system is the FM exchange between Co ions in the B position. The

ordering of Gd ions in the A position is weakly affected by this exchange. At the same time, the ordering of oxygen vacancies and, therefore, the spatial distribution of magnetically active Co ions in the pyramidal environment play a crucial role in the magnetic state of the system against the background of the growing magnetic contribution of Co^{3+} ions to the octahedral environment involved in the LS $\rightarrow$ (HS/IS) spin crossover. All physical quantities investigated in this work showed clearly pronounced anomalies at 260 K and 360 K for disordered and ordered samples, respectively.

The X-ray absorption spectra indicate that the method of charge compensation in the cobaltites under study is more complex than expected based on analogy with manganites [27]. Along with a change in the electronic state of cobalt there is a partial change in the charge state of oxygen ions. If we assume that, in accordance with the requirement of preserving the local electroneutrality, the holes in the O2*p* states are localized near the Gd^{3+}/Sr^{2+} substitution sites, that is, in the $[Gd_{0.1}Sr_{0.4}O_{0.5-0.4\delta}]$ planes, there should be a correlation between the spatial distribution of Gd^{3+}/Sr^{2+} and oxygen holes O2*p*. In the case of GSC-dis samples, this distribution is random, and for GCS-ord samples there are signs of a certain order. The oxygen hole can make an additional contribution to magnetization as an independent paramagnetic center or participate in the exchange coupling with magnetic Gd and Co ions, creating exchange-coupled magnetic complexes.

ACKNOWLEDGMENTS

The authors are grateful to L.A. Solov'ev for providing X-ray diffraction data and to M.S. Platunov for assistence in measurements of X-ray spectra.

FUNDING

This work was supported by the Russian Foundation for Basic Research (grant nos. 17-02-00826, 16-02-00507, and 18-52-00017 Bel_a) and by the Council on Grants of the President of the Russian Federation (SP-1844.2016.1). X-ray spectra were recorded using the equipment of a unique scientific facility Kurchatov Synchrotron Radiation Source financed by the Ministry of Education and Science of the Russian Federation (project ID RFMEFI61917X0007).

REFERENCES

1. N. B. Ivanova, S. G. Ovchinnikov, M. M. Korshunov, I. M. Eremin, and N. V. Kazak, Phys. Usp. **52**, 789 (2009).
2. M. James, L. Morales, and K. Wallwork, Phys. B (Amsterdam, Neth.) **199**, 385 (2006).
3. M. James, T. Tedesco, D. J. Cassidy, and R. L. Withers, Mater. Res. Bull. **40**, 990 (2005).
4. I. O. Troyanchuk, D. V. Karpinsky, M. V. Bushinsky, V. Sikolenko, V. Efimov, A. Cervellino, and B. Raveau, J. Appl. Phys. **112**, 013916 (2012).
5. A. M. Balagurov, I. A. Bobrikov, D. V. Karpinsky, I. O. Troyanchuk, V. Yu. Pomyakushin, and D. V. Sheptyakov, JETP Lett. **88**, 531 (2008).
6. S. N. Vereshchagin, L. A. Solovyov, E. V. Rabchevskii, V. A. Dudnikov, S. G. Ovchinnikov, and A. G. Anshits, Chem. Commun. **50**, 6112 (2014).
7. R. Liu, Y. Xuan, and Y. Q. Jia, Mater. Chem. Phys. **57**, 81 (1998).
8. L. Mogni, F. Prado, C. Jiménez, and A. Caneiro, Solid State Ionics **240**, 19 (2013).
9. Q. Yin and Y. S. Lin, Solid State Ionics **178**, 83 (2007).
10. Z. H. Yang and Y. S. Lin, Solid State Ionics **176**, 89 (2005).
11. V. A. Dudnikov, S. G. Ovchinnikov, Yu. S. Orlov, N. V. Kazak, K. R. Michel, G. S. Patrin, and G. Yu. Yurkin, J. Exp. Theor. Phys. **114**, 841 (2012).
12. S. G. Ovchinnikov, Yu. S. Orlov, V. A. Dudnikov, S. N. Vereshchagin, and N. S. Perov, J. Magn. Magn. Mater. **383**, 162 (2015).
13. R. D. Shannon, Acta Crystallogr., A **32**, 751 (1976).
14. M. S. Platunov, V. A. Dudnikov, Yu. S. Orlov, N. V. Kazak, L. A. Solovyov, Ya. V. Zubavichus, A. A. Veligzhanin, P. V. Dorovatovskii, S. N. Vereshchagin, K. A. Shaykhutdinov, and S. G. Ovchinnikov, JETP Lett. **103**, 196 (2016).
15. Yu. S. Orlov, V. A. Dudnikov, M. V. Gorev, S. N. Vereshchagin, L. A. Solov'ev, and S. G. Ovchinnikov, JETP Lett. **103**, 607 (2016).
16. J. W. Visser, J. Appl. Crystallogr. **2**, 89 (1969).
17. H. M. Rietveld, J. Appl. Crystallogr. **2**, 65 (1969).
18. L. A. Solovyov, J. Appl. Crystallogr. **37**, 743 (2004).
19. K. Conder, E. Pomjakushina, A. Soldatov, and E. Mitberg, Mater. Res. Bull. **40**, 257 (2005).
20. O. Haas, R. Struis, and J. M. McBreen, J. Solid State Chem. **177**, 1000 (2004).
21. G. Thornton, I. W. Owen, and G. P. Diakun, J. Phys.: Condens. Matter **3**, 417 (1991).
22. M. G. Kim, Y. S. Im, E. J. Oh, K. H. Kim, and C. H. Yo, Phys. B (Amsterdam, Neth.) **229**, 338 (1997).
23. V. A. Dudnikov, D. A. Velikanov, N. V. Kazak, C. R. Michel, J. Bartolome, A. Arauzo, S. G. Ovchinnikov, and G. S. Patrin, Phys. Solid State **54**, 79 (2012).
24. N. B. Ivanova, J. Bartolomé, A. Figueroa, J. Blasco, A. Arauzo, M. S. Platunov, V. V. Rudenko, and N. V. Kazak, Solid State Phenom. 168-–169, 501 (2011).
25. T. N. Vasil'chikova, T. G. Kuz'mova, A. A. Kamenev, A. R. Kaul', and A. N. Vasil'ev, JETP Lett. **97**, 34 (2013).
26. Z. Hu, Hua Wu, M. W. Haverkort, H. H. Hsieh, H.-J. Lin, T. Lorenz, J. Baier, A. Reichl, I. Bonn, C. Felser, A. Tanaka, C. T. Chen, and L. H. Tjeng, Phys. Rev. Lett. **92**, 207402 (2004).
27. M. Yu. Kagan and K. I. Kugel', Phys. Usp. **44**, 553 (2001).

Translated by Andrey Zeigarnik